

New dynamic semiconductor laser model based on the transmission-line modelling method

A.J. Lowery, BSc

Indexing terms: Semiconductor lasers, Optoelectronics, Modelling

Abstract: A versatile semiconductor laser model has been developed by the addition of a frequency-dependent gain model to the transmission-line modelling (TLM) method. The model provides a sampled optical output waveform for a modulated laser, from which output spectra may be found. To minimise computing time, a technique of sampling below the optical frequency is introduced. The theoretical basis for this model is considered, and the results gained for a 300 μm cavity heterojunction laser are compared with those given by the solution of the rate equations.

1 Introduction

The operation of a semiconductor laser provides an extremely complex modelling problem. A complete model would include the solution of optical field and carrier diffusion equations in a three-dimensional (3D) dielectric waveguide whose dimensions may be carrier dependent. The dielectric's refractive index would include real and imaginary components, both being functions of wavelength and carrier density. Also, as the semiconductor laser's major role is as a modulated source in optical communications, it is necessary to have a dynamic rather than static model of its operation.

The limitation of computing power has made the above model impossible to realise [1]. However, many models are available, all of which concentrate on one aspect of the laser's operation, for example transverse field and carrier distribution [2], or laser linewidth [3]. To design a laser, the individual models must be spliced together, which may be a long-winded process and prone to error.

This paper introduces a new type of semiconductor laser model based on the transmission-line modelling (TLM) method. This method has been used extensively to model both field and diffusion problems [4, 5] and produces stable, explicit and easy-to-understand routines. This model is not intended to be a complete model of the lasing process, but the approach is designed to be adaptable to individual requirements and novel device structures. This paper serves as an introduction to the technique and, for comparison with other techniques, concentrates on the modelling of transient spectra.

Paper 5608J (E13), first received 2nd December 1986 and in revised form 13th March 1987

The author is with the Department of Electrical and Electronic Engineering, The University of Nottingham, University Park, Nottingham NG7 2RD, United Kingdom

The evolution of the laser spectrum under modulation is required to determine the dispersion in fibres and thus maximise the bandwidth-length product [6]. Many models concentrate on this feature, and particularly on the increase in linewidth under modulation. A common approach is to solve a set of rate equations for photon and carrier density, using one rate equation per longitudinal mode [7–10]. The evolution of the relative mode powers during a modulation pulse is then found using some form of numerical solution.

The fundamental difference between the transmission-line laser model (TLLM) and the above rate-equation models is that the TLLM discretises the rate equations in space rather than wavelength. This is achieved by using a field model for the laser cavity to deal with the wavelength dependence of the gain. It will be shown that the number of sections required equals the number of longitudinal modes to be modelled. One advantage is that spatial inhomogeneities are included without adding extra rate equations. Another advantage is that the wavelength spectrum is continuous, allowing longitudinal modes to fractionally shift, as in the real device [11].

Besides the output spectrum, another important device parameter is its input impedance. This is required for the design of drive electronics and to assess the effects of parasitic components. The equivalent-circuit class of models, reviewed in Reference 12, allows the laser processes to be represented by a network of standard components. This may then be appended to models of the device package and drive circuit to obtain a complete transmitter model.

In comparison, the availability of a TLM for lumped components [13] allows the TLLM to include external and parasitic components, justifying the TLLM as an equivalent-circuit model. The important difference is that the TLLM includes a cavity model. This allows novel structures to be investigated and, more fundamentally, provides the optical waveform, whereas the others only provide the power envelope.

The following Sections aim to describe the additions required to the TLM method for waveguide problems to form a laser model. The technique will then be tested against other models by using a 300 μm stripe GaAlAs laser as an example.

2 Optical cavity

The basis of a semiconductor laser is a guiding optical cavity filled with a medium which provides optical gain at the lasing frequency and whose end facets are mirrored to provide positive optical feedback [14]. The guiding may be provided by a built-in refractive-index step, known as 'index guiding', or by modulation of the refractive index by current injection, 'gain guiding'. The latter

is difficult to model as the cavity dimensions are a function of local carrier concentration. The former, however, has fixed cavity dimensions, although refractive-index modulation may occur, and so the waveguide dispersion and confinement can be considered as being constant. Thus, it is possible to reduce the model to one dimension, along the cavity. This type of laser is considered in this paper.

The co-ordinate system is shown in Fig. 1 together with cavity dimensions, which are detailed later in the paper.

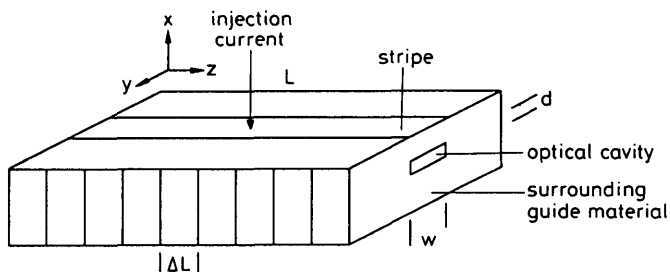


Fig. 1 Stripe geometry semiconductor laser with built-in waveguiding

The optical wave is usually thought of as propagating as a TE_{10} mode, with its electric field $E_y(x, y, z, t)$ in the y -direction. For a one-dimensional (1D) model the x and y dependence have to be removed. This is achieved by averaging the field over all x and y and equating its power to that of a field $E(z, t)$ over an area wd , where w is the stripe width and d is the guide thickness:

$$|E(z, t)|^2 = \frac{1}{wd} \int_{-\infty}^{\infty} \int_{-\infty}^{\infty} |E_y(x, y, z, t)|^2 dx dy \quad (1)$$

The magnitude of $E(z, t)$ may be related to the photon density $S(z, t)$ in the cavity by noting that the power density across our chosen cavity area equals the energy density multiplied by the group velocity. Thus:

$$\frac{|E(z, t)|^2}{Z_p} = S(z, t) \frac{hc^2}{\lambda_0 \bar{n}_e} \quad (2)$$

Where h = Planck's constant (6.626×10^{-34} Js)
 c = vacuum velocity of light (3×10^{10} cms $^{-1}$)
 λ_0 = laser's free-space wavelength
 \bar{n}_e = effective group index

Z_p is the transverse wave impedance for a TE mode, in a guide of effective index n_e [15], given by:

$$Z_p = \bar{n}_e 120\pi/n_e^2 \quad (3)$$

The propagation of $E(z, t)$ along the cavity will now be modelled using the TLM method.

3 Representation of optical electric field

The longitudinal variation of optical field is modelled by using the standard TLM method for waveguides, introduced by Johns and Beurle [16], reduced to one dimension. The cavity, length L , is split into s sections each of length ΔL . For subNyquist operation ΔL must be less than one half of the group wavelength λ_{gr} . This condition will be used, for simplicity, to develop the TLLM. The modelling speed may be greatly enhanced by sampling below the Nyquist limit [17], and the necessary modifications are described in Section 8.

The group wavelength is related to the free-space wavelength λ_0 by

$$\lambda_{gr} = \frac{\lambda_0}{\bar{n}_e} \quad (4)$$

Thus, the minimum number of sections is given by

$$s = \frac{2L\bar{n}_e}{\lambda_0} \quad (5)$$

The TLM method represents each section by a transmission line, the voltage on the line representing, in this case, the transverse electric field in the cavity. To discretise time, voltage pulses travel along the sections at intervals of ΔT . The sections are jointed at nodes, at which incident voltage pulses will be scattered to become reflected pulses out of the nodes. ΔT is such that a reflected pulse out of one node will become an incident pulse on the adjacent node at the next iteration, i.e.

$$\Delta T = \frac{\Delta L \bar{n}_e}{c} \quad (6)$$

The phase velocity along the transmission lines is used to model the group velocity in the cavity. This is because the group velocity is required to give the correct longitudinal mode spacing, and the TLM cavity model is dispersionless, i.e. its group velocity equals its phase velocity. This condition is also required when the solution of the rate equations is considered.

To model refractive-index changes along the cavity, the velocity along the transmission line may be altered by including capacitive transmission-line stubs at the connection nodes [18]. These serve to alter the phase velocity along the line. The study of these, and the modelling of laser chirp, is beyond the scope of this paper.

The end facets are simply modelled by using unmatched termination resistors at the end nodes of the cavity. It is assumed that there is zero back scatter into the cavity, for example from the fibre end face. However, this may be easily modelled by extending the transmission-line sections beyond the cavity. Buus [19] provides a simple analytical method of determining the reflectance of uncoated end facets.

4 Representation of gain curve

The 1D cavity described in Section 3 can only model changes in the real part of the refractive index along the cavity length. The frequency response of the cavity could be found by injecting an impulse into one node and taking a Fourier transform of the resulting stream of pulses at a chosen node. The response for a homogeneous cavity would be composed of equally spaced 'longitudinal modes' of equal amplitude.

The above model takes no account of the imaginary part of the refractive index, which results in materials gain or loss. This term is wavelength dependent and so serves to select one or more of the longitudinal modes to become the dominant laser mode. Thus some form of wavelength-dependent amplification is required in the cavity.

The magnitude of this amplification may be found by using the rate equation for photon density, originally derived by Statz and DeMars [20]. The facet reflectivity terms are neglected as their contribution is modelled by

unmatched terminations. The rate equation becomes

$$\frac{dS}{dt} = \frac{cS}{\bar{n}_e} (g\Gamma - \alpha_{sc}) + \frac{N\beta}{\tau_s} \quad (7)$$

Where S = photon density
 Γ = confinement factor
 g = spatial gain coefficient
 α_{sc} = internal loss coefficient
 β = spontaneous coupling coefficient
 τ_s = carrier lifetime
 N = carrier concentration

Neglecting the spontaneous emission term for the time being, consider the increase in photon density between two nodes ΔL apart. This may be found using eqns. 6 and 7:

$$\frac{S_{\Delta L}}{S_0} = \exp \Delta L(\Gamma g - \alpha_{sc}) \quad (8)$$

As the magnitude of the transverse electric field E is proportional to the square root of photon density, assuming a monochromatic beam, then

$$\frac{E_{\Delta L}}{E_0} = \exp \Delta L(\Gamma g - \alpha_{sc})/2 \quad (9)$$

The internal loss term is assumed to be frequency independent and may be represented by an attenuator with an attenuation of $\exp(\alpha_{sc} \Delta L/2)$. The remaining exponential may be expanded to a Taylor series:

$$\frac{E_{\Delta L}}{E_0} = \left(1 + \frac{\Delta L \Gamma g}{2}\right) \exp(\alpha_{sc} \Delta L/2) \quad (10)$$

This equation suggests the model shown in Fig. 2. The wavelength dependence of the gain curve may be represented by a passive filter, which is discussed in the following Section.

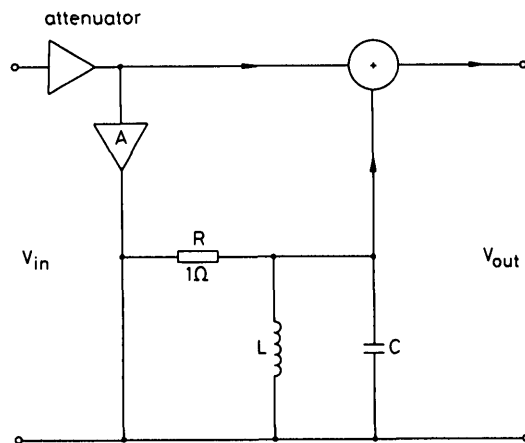


Fig. 2 Gain curve model

represented by a passive filter, which is discussed in the following Section.

5 Frequency dependence of gain curve

The gain curve may be found theoretically, e.g. Stern [21], Mendoza *et al.* [22], or experimentally, e.g. Henry *et al.* [23]. It is usually given in the form of a series of frequency-dependent curves, each for a certain carrier concentration. The model described in this paper approximates the curve to a Lorentzian form so that a simple second-order bandpass filter may be used. This approximation has been used by Lau and Yariv [24] as a good fit is obtained at the peak of the gain curve, around which most of the laser power is produced.

The inductor and capacitor, required for the second-order filter, are modelled by using transmission-line stubs. These stubs are joined with the resistor at a node. This technique is described by Johns and O'Brien [13]. The stubs are made of such a length that a pulse reflected into them will become an incident pulse at the node one time step later. By comparing the input impedance of an open-circuited transmission-line stub with that of a capacitor value C , it can be shown that the capacitor may be represented by a stub of impedance Z_c , where

$$C = \frac{\Delta T}{2Z_c} \quad (11)$$

Similarly, a short-circuited stub of impedance Z_L may represent an inductor value L :

$$L = \frac{Z_L \Delta T}{2} \quad (12)$$

These approximations hold while the time step is much less than the period of the wave. For computational speed reasons, this is not the case with our model. A better method of calculating the stub impedances is developed by considering the input impedances of the stubs, which are, for the capacitive stub:

$$Z_{ic} = Z_c/j \tan(\pi \cdot \Delta T \cdot c/\lambda_0) \quad (13)$$

and for the inductive stub:

$$Z_{il} = Z_L j \tan(\pi \cdot \Delta T \cdot c/\lambda_0) \quad (14)$$

At resonance, the parallel combination of stub admittance is zero, giving a relation between resonant wavelength and stub impedances:

$$\sqrt{Z_c/Z_L} = \tan(\pi \cdot \Delta T \cdot c/\lambda_0) \quad (15)$$

This relation shows the existence of higher-order passbands (argument of $\tan > 2\pi$) which can be used when the time step is increased beyond the Nyquist sampling theorem limit.

The Q -factor of a parallel RLC filter, whose R value is unity, is given by

$$Q = \sqrt{C/L} \quad (16)$$

The Q -factor of the TLM stub filter can be found by substituting for L and C :

$$Q = 1/\sqrt{Z_c/Z_L} \quad (17)$$

An amplifier, gain A , is used to define the gain at resonance of the network shown in Fig. 2. For a laser the gain is a function of excess carrier concentration and may be approximated to [1]

$$g = B(N - N_{tr}) \quad (18)$$

Where B = spatial gain per unit carrier density

N = carrier density

N_{tr} = carrier density for transparency

The gain of the amplifier is therefore

$$A = \frac{\Delta L}{2} \Gamma B(N - N_{tr}) \quad (19)$$

The filter is now fully defined. Two filter 'modules' are required between adjacent nodes, one for each pulse direction. This is a requirement of the conservation of photon momentum, i.e. photons created by stimulated emission are emitted in the same mode and in the same phase as the photon stimulating the transition.

It should be noted that the filter introduces a phase shift to the wave. This is related to the amplitude

response by the Kramers-Kronig [25] relations. These also relate gain and refractive index in the laser, and so it can be shown that the filter serves a dual purpose, i.e. if the gain curve is accurately modelled, the refractive-index variations will also be modelled. For example, this effect may be used to model frequency chirping [11].

6 Modelling spontaneous emission

The last term in the photon density rate equation (eqn. 7) covers the photons added by spontaneous emission. The rate of photon creation is proportional to the carrier concentration N , the effective cavity volume $w dL$ and the inverse of carrier lifetime τ_s . If the mean energy of the photons is hf_{res} , where $f_{res} = c/\lambda_0$, then the spontaneous emission power becomes

$$P_{sp} = \beta \frac{N}{\tau_s} hf_{res} w dL \quad (20)$$

The spontaneous emission coupling coefficient β is included as not all photons thus created have the correct wave vector to be coupled to the guided wave.

This power may be injected into the model at each section or, to save on computing time, may be localised to one section. This approach may be justified if the spontaneous emission spectra are measured assuming a localised source [26].

As spontaneous emission is a random process, a random noise source is used as a model. To obtain the correct noise spectrum, a Gaussian (normal) distribution discrete source, with zero mean, is filtered by a second-order RLC filter similar to that used for the gain curve model.

The RMS output of the filtered source is equal to its variance multiplied by the effective bandwidth of the filter over the Nyquist bandwidth, i.e.

$$E_{rms}^2 = \sigma^2 2 \Delta T B_e \quad (21)$$

The effective bandwidth B_e is found by integration of the filter's response over all positive frequencies. The RLC filter has a Lorentzian response $H(\omega)$, where

$$H(\omega) = \frac{\omega_0^2}{4Q^2} \left/ \left((\omega - \omega_0)^2 + (\omega_0/2Q)^2 \right) \right. \quad (22)$$

Where ω is the angular frequency and ω_0 equals $2\pi f_{res}$. The effective bandwidth is $\omega_0/4Q$ Hz. If the filtered source is used as a voltage source in the model, representing field in the laser cavity, then the power of the source becomes

$$P = \frac{\omega_0 \sigma^2 \Delta T w d}{2QZ_p} \quad (23)$$

Equating this power with the spontaneous emission power to find the required variance gives

$$\sigma^2 = \frac{\beta N h L Q Z_p}{\pi \Delta T \tau_s} \quad (24)$$

The voltage output of the filter is simply added to the voltage on the transmission line, at one node, in one wave direction. The carrier concentration N in the cavity should be calculated from the mean concentration of all the sections.

As with the gain curve, the spontaneous emission spectrum is a function of carrier concentration. The central resonance of the filter could be made a function of concentration to cater for this effect.

7 Modelling the rate equation for carrier concentration

The preceding Sections in this paper have been concerned with the solution of the rate equation for photon density. This included terms for carrier concentration. This Section of the paper involves the modelling of the rate equation for carrier concentration so that the two equations may be solved simultaneously.

The rate equation for carrier concentration may be written

$$\frac{dN}{dt} = \frac{j}{ed} - \frac{N}{\tau_s} - \frac{c}{\bar{n}_e} \Gamma g S \quad (25)$$

Where j is the injection current density and e is the charge of an electron.

To enable longitudinal carrier density variation to be modelled, an independent rate equation is used for each model section. s may be found from the reflected voltages in the cavity model by using eqn. 2 and noting that voltage is equivalent to the transverse effective electric field.

An equivalent circuit may be constructed where voltage represents carrier density, as in Fig. 3. The differential equation for this is

$$\frac{dQ}{dt} = I_{inj} - \frac{V}{R_3} - I_{stim} \quad (26)$$

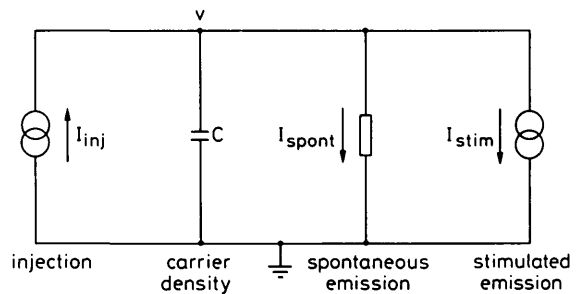


Fig. 3 Carrier rate-equation model

For the capacitor $Q = CV$. For convenience $C = 1$. Equating coefficients gives

$$I_{inj} \equiv \frac{j}{ed} \quad (27)$$

$$R_3 \equiv \tau_s \quad (28)$$

$$I_{stim} \equiv \frac{c}{\bar{n}_e} \Gamma g S \quad (29)$$

As before, a TLM stub is used to model the capacitor. The effect of stray components is negligible as the time constant of this circuit is far longer than the time step. The complete photon and carrier model is shown in Fig. 4.

Diffusion along the cavity has so far been neglected as it is negligible for lasers with uncoated (high reflectivity) facets. If required, diffusion may be modelled by linking the model sections with resistors. An explicit routine, using link transmission-line sections, is suggested by Johns [27].

8 Sampling theory

The Nyquist theorem [17] states that if a signal, band-limited to B Hz, is sampled at a rate of $2B$ samples per

second, the signal may be recovered without loss of information. So far a sampling rate of at least twice the optical frequency f_{res} has been used, allowing signals from DC to the laser's optical frequency to be recovered.

With this method much of the available spectrum remains unused, as the laser's spectrum is very narrow ($\approx 10^{12}$ Hz) compared with its operating frequency ($\approx 10^{14}$ Hz). This fact suggests that the sampling rate may be lowered without loss of information.

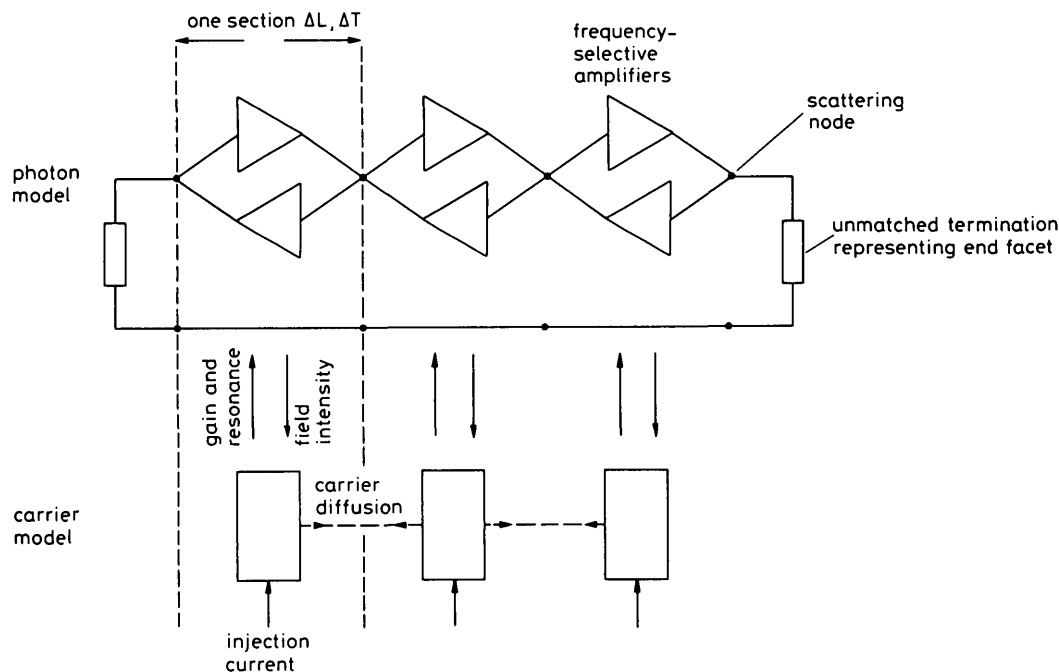


Fig. 4 1D transmission-line model of a semiconductor laser

Consider the laser output to lie within a band $f(min)$ to $f(max)$. Let the sampling rate be $f(samp)$. The band will be replicated around DC and all harmonics of $f(samp)$. To reduce modelling time $f(samp)$ has to be minimised without information loss in the band. This is achieved when $f(min)$ is replicated at zero frequency (DC), by sampling at $f(min)/b$, where b is an integer and will be referred to as the band number. This replication is shown in Fig. 5. To prevent overlapping of the bands, $f(samp)$

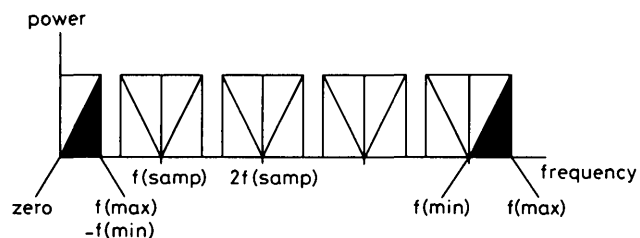


Fig. 5 Replication of a band $f(min)$ to $f(max)$ at zero to $f(max) - f(min)$

must be greater than $2(f(max) - f(min))$. Combining these two limits provides a maximum value for the band number:

$$b \leq f(min)/(2f(max) - 2f(min)) \quad (30)$$

Owing to the nature of the model, an integer number of sections s is required along the cavity. This puts a constraint on $f(min)$, which has to be chosen such that

$$f(min) = sbc/(L\bar{n}_e) \quad (31)$$

Similarly $f(max)$ is given by

$$f(max) = s(b + 1/2)c/(L\bar{n}_e) \quad (32)$$

Obviously $f(min)$ is chosen to be below the region of interest, and $f(max)$ is chosen to be above it. It is interesting to note that $f(min)$ and $f(max)$ both fall on longitudinal modes, which are spaced at $c/2L\bar{n}_e$ (neglecting material dispersion), and that the number of sections

equals the number of longitudinal modes that will be modelled.

There are two other factors governing the choice of s . These are the accuracy of the Taylor series expansion and the accuracy of the diffusion model. First, let us consider the Taylor series expansion of the gain curve. In the steady state, the material gain has to compensate for both mirror loss and material absorption [28]. If mirror loss is considered dominant and has a value R for both mirrors, the spatial gain coefficient multiplied by the confinement factor becomes

$$g\Gamma = -\frac{1}{L} \ln(R) \quad (33)$$

This figure is then substituted into eqn. 9 to find the increase in field per section. This is then raised to the power $2s$ to find the model gain over the entire cavity length, giving

$$\frac{P_L}{P_0} = \left(1 + \frac{gL\Gamma}{2s}\right)^{2s} \quad (34)$$

The model gain over the required gain ($1/R$) against reflectivity is plotted in Fig. 6.

It should be noted that in the dynamic situation the peak gain can be up to five times the steady-state value, which gives a considerably larger error. This results in an increased turn-on time owing to the reduced gain at high carrier density levels.

Secondly, the section length should be kept below the diffusion length for accurate modelling of spatial hole burning effects [1]. As this paper considers lasers with high-reflectivity facets, the carrier concentration variation

along the cavity is small, and hence diffusion effects have been ignored. However, if the model is to be used for low-reflectivity situations, such as with laser amplifiers,

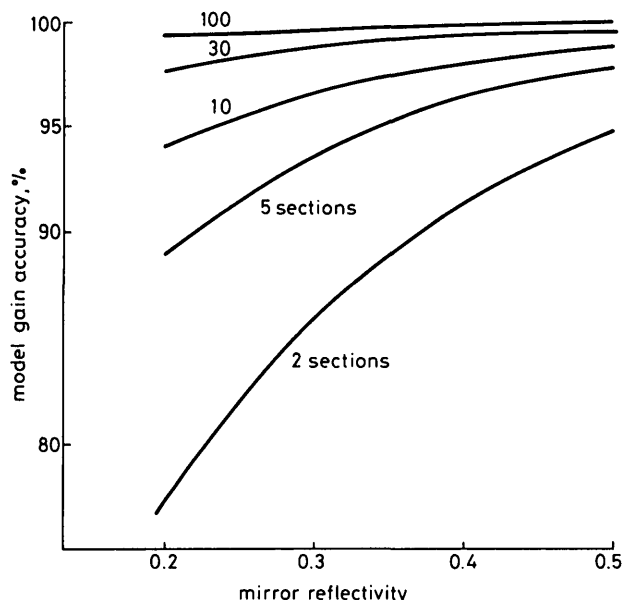


Fig. 6 Accuracy of Taylor series expansion

the diffusion model, and hence the choice of s , require careful consideration.

Once the band number and number of sections have been determined, the following model parameters have to be recalculated:

(a) *Gain curve filters*: The bandwidth of the curve is to be kept constant so that the same number of longitudinal modes lie under it. This implies that the 'Q' of the filters has to be decreased as $Q = \text{resonant frequency}/\text{bandwidth}$. Formally, if $Q(gc)$ is the Q-value of the gain curve and $Q(fil)$ is the Q-value of the stub filters, then

$$Q(gc) = Q(fil)(1 - bf(samp)/f(res)) \quad (35)$$

(b) *Fourier transform*: The resolution ΔF of an r -point discrete Fourier transform will be

$$\Delta F = f(samp)/r \quad (36)$$

For the individual modes to be resolved, the resolution of the transform has to be made less than the longitudinal mode spacing. By relating the mode spacing to the number of sections it can be shown that

$$r \geq 2s \quad (37)$$

The transform is only valid in the range $f(\min)$ to $f(\max)$.

(c) *All occurrences of ΔL and ΔT* : In every case, the newly calculated section length and time step should be substituted into the original equations. These are given by

$$\Delta L = L/s \quad (38)$$

$$\Delta T = 1/d(samp) \quad (39)$$

9 Modelling speed

It is useful to put a measure on the speed improvement gained by sampling below the Nyquist rate and also to be able to compare the TLLM method with other laser models in terms of speed. In this Section the modelling of a 300 μm laser operating at 850 nm with a group index of four will be used as a benchmark. If sampling above

the Nyquist rate is used, eqn. 5 gives the minimum number of sections as 3000.

A useful measure of computations required per nanosecond of laser time is $10^{-9} s/\Delta T$, the number of node iterations per nanosecond. Thus, 2000 million node iterations are required for a nanosecond of laser time. A Whitechapel MG1 workstation takes about 1.4 ms per node iteration, giving a computation time of 800 h/ns.

For subNyquist sampling the modelling time is more realistic. If s is the number of sections chosen, the number of node iterations per nanosecond ($nins$) becomes

$$nins = \frac{s^2 c \times 10^{-9}}{L \bar{n}_e} \quad (40)$$

Our example, using 100 sections, requires 2.5 million node iterations per nanosecond, giving a modelling time of around 60 minutes. A multimode rate-equation model [7] with an equal bandwidth and an iteration time step of 0.5 ps takes 1.6 minutes. However, if spatial variations are to be included, the computing time will be increased in proportion to the number of sections, and for 100 sections the TLM model is more than twice as fast as the rate-equation model.

10 Modelling transient response of a laser

The TLM model is primarily a dynamic model, i.e. the laser is being modulated. However, it may be used as a static model if the injection current is kept constant and the model is allowed to reach a steady state. To minimise the settling time, the initial value of carrier concentration can be set to the threshold carrier concentration.

The dynamic response may be found by applying a step (or otherwise) input of injection current. If the step is from a nonzero current value, e.g. the laser is biased below threshold, then the model should strictly be allowed to stabilise before the step is applied.

The electric field may be sampled at any point along the model. However, it is usually sampled just inside the end facets. The result will be a series of impulses, one per iteration. The instantaneous output power is simply given by the instantaneous power density incident on the facet multiplied by $(1 - R)$, that is:

$$P(t) = \frac{E^2(t)}{Z_p} (1 - R)wd \quad (41)$$

The average output power may be found by averaging over a number of wave periods, noting that the longitudinal modes will beat at their difference frequency.

11 Comparing the model to a simple solution of the rate equations

To verify the operation of the model, a hypothetical laser was analysed using TLM, a numerical solution of the rate equations [7] and a small signal analysis of the rate equations [28, 29]. Table 1 shows the laser parameters. The assumptions are as follows:

- (i) zero carrier diffusion
- (ii) homogeneous transverse wave impedance
- (iii) spontaneous emission spectrum equals gain spectrum
- (iv) above spectra independent of carrier concentration
- (v) carrier lifetime independent of carrier concentration

The model parameters were then calculated by the use of the equations derived in this paper and are shown in

Table 1: Modelled laser parameters

Symbol	Parameter	Value
λ_0	Free-space wavelength	850 nm
L	Cavity length	300 μm
\bar{n}_e	Group index	4
n_e	Effective index	3.5
R_1, R_2	Facet reflectivities	0.3
Q	Gain curve Q -factor	100
$B\Gamma$	Gain constant \times confinement factor	$1.5 \times 10^{-16} \text{ cm}^2$
N	Transparency carrier density	$1.5 \times 10^{18} \text{ cm}^{-3}$
d	Active region depth	0.1 μm
w	Stripe width	5 μm
τ_s	Carrier lifetime	4 ns
a_{sc}	Internal attenuation	10 cm^{-1}
β	Spontaneous emission coupling factor	0.01

Table 2. The frequency response of one filter section was

Table 2: Model parameters

Symbol	Parameter	value
b	Band number	14
s	Actual number of sections	100
$f(\text{samp})$	Sampling frequency	$2.5 \times 10^{13} \text{ Hz}$
ΔT	Timestep per iteration	40 fs
ΔL	Section length	3.0 μm
$Q(\text{new})$	Modified Q -factor	0.83333
Z_c	Impedance of stub capacitor	4.43513 Ω
Z_L	Impedance of stub inductor	32.46803 Ω
Z_p	Cavity wave impedance	123.1 Ω
Att	Attenuation per section	0.998501
R	Spontaneous emission resistor	$4 \times 10^{-9} \Omega$
r	Number of transform points	1024
ΔF	Transform resolution	25 GHz
$\Delta \lambda$	Transform resolution	0.06 nm

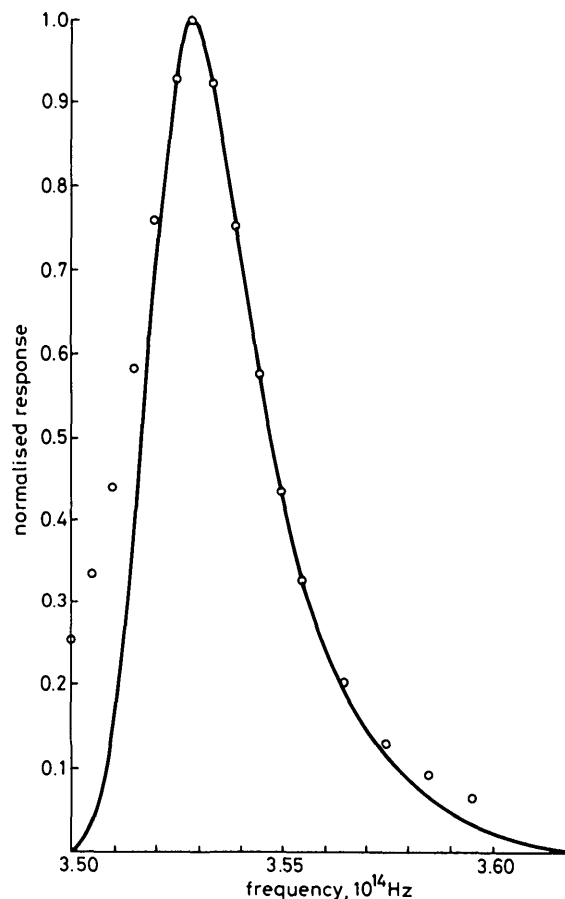
checked against the expected Lorentzian response, and both are shown in Fig. 7. As the modelled band has been translated down in frequency by $f(\text{min})$, the response falls to zero at this frequency. However, the filter response is a good fit at the important resonance peak. The model was then tested under a number of conditions, the results of which are analysed as follows:

11.1 Interaction of photon and carrier populations

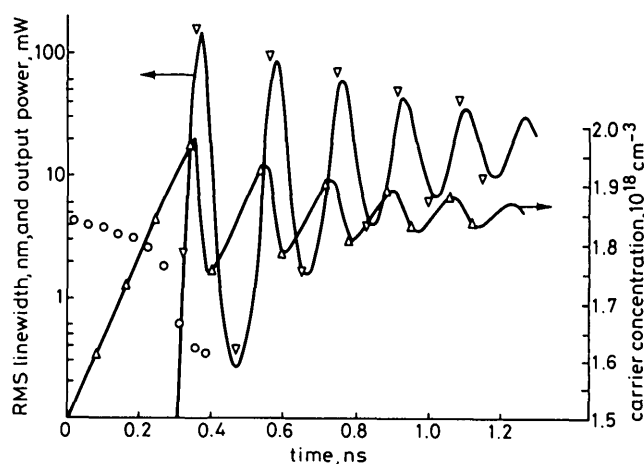
The interaction of photon and carrier concentrations for a step increase in injection current to 44 mA has been modelled using TLM and a multimode numerical solution to the rate equations. The results are shown in Fig. 8 which also includes a plot of RMS linewidth calculated from the former model. Both models use the parameters in Table 1, except that the latter's spontaneous emission coupling factor has been reduced to 0.0001 to achieve matching between the oscillation amplitudes. This discrepancy is due to the definitions of the coupling factors. The TLM model splits the spontaneous emission power multiplied by the coupling factor over the lasing bandwidth; whereas the rate-equation model splits the coupled power between the modes. Thus more power reaches the modes in the latter situation, giving greater damping of the oscillations.

When the current step is applied, the carrier concentration rises from the transparency value, increasing material gain from zero. The power output, which is initially dominated by spontaneous emission noise, rises at an increasing rate as stimulated emission becomes dominant. This transition can also be seen by comparing Figs. 9a and 9b, the spectra at 0.22 and 0.34 ns. The

former shows a broadband output, comprising multiple longitudinal modes within the spontaneous emission envelope. The latter shows a narrower spectrum composed of four distinct modes, with little noise power in between them.

**Fig. 7** TLM stub filter and Lorentzian filter responses

— TLM stub filter response
 ○ ○ ○ Lorentzian response

**Fig. 8** Transient response of a 300 μm stripe laser driven with a current step of 44 mA

— TLM model results
 $\Delta \Delta \Delta$ multimode rate-equation results
 ○ ○ ○ linewidth

At around 0.35 ns the stimulated recombination rate becomes greater than the injection rate, resulting in a dramatic decrease in carrier concentration to below the threshold required to maintain a constant photon density. The output power falls, allowing carrier concentration to rise. The interaction of carrier and photon densities continues until a near steady state is obtained. The

laser now operates with two dominant modes, whose relative amplitudes remain constant, as shown in Figs. 9c and 9d; the spectra at 0.5 and 1 ns. The linewidth of each mode is now less than the transform resolution, and the RMS linewidth falls below 0.5 nm.

12 Discussion

The results given in the preceding Section show that the concept and derivation of the 1D transmission line laser model (TLLM) are sound. The model is able to predict the evolution of output spectra during a transient and

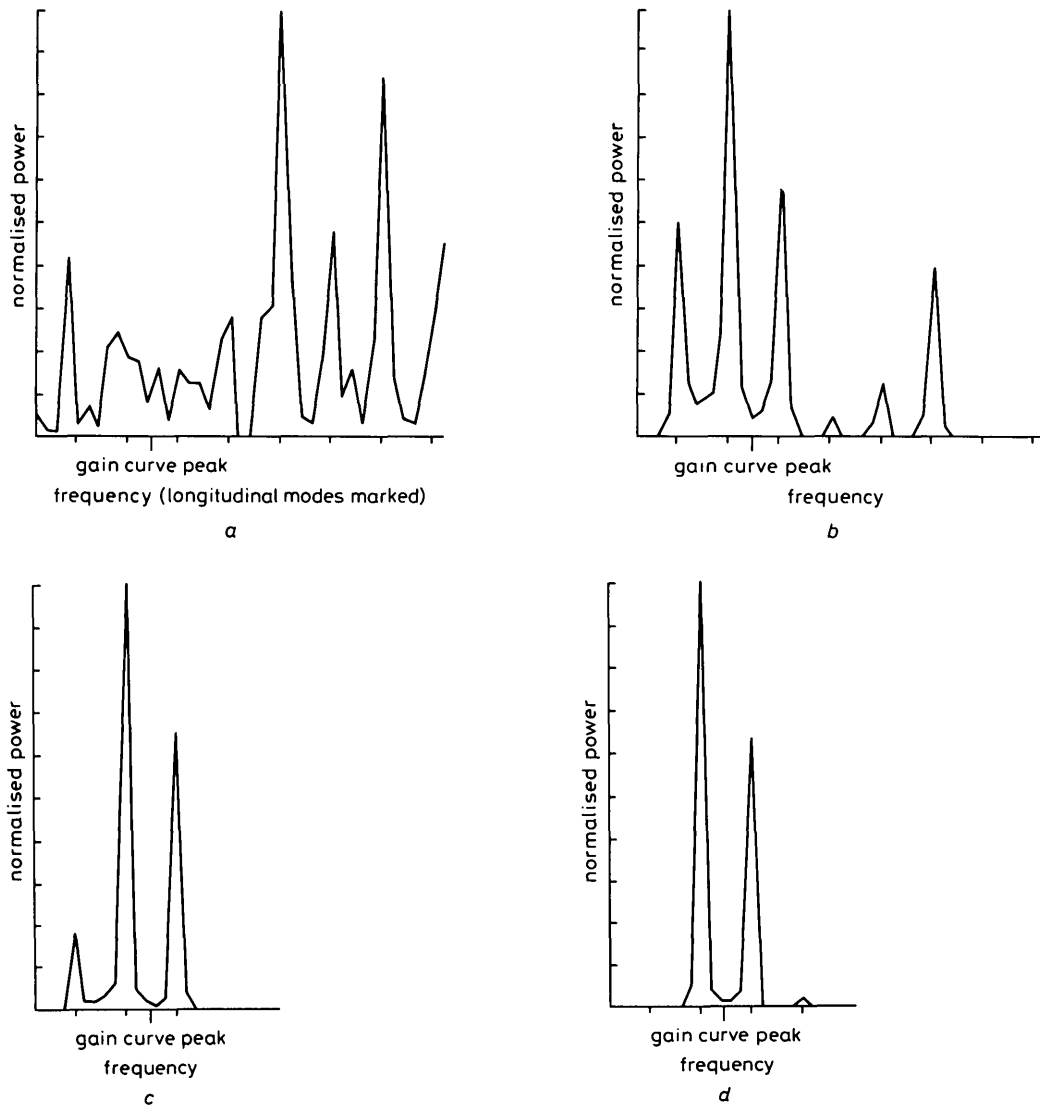


Fig. 9 Modelled spectra during the turn-on transient shown in Fig. 8
a 0.22 ns b 0.34 ns c 0.5 ns d 1 ns

11.2 Power output, delay time and resonance frequency against drive current

A small signal analysis of the rate equations provides equations for resonance frequency, turn-on delay and output power [28]. These are compared with the model at a number of drive currents, as shown in Fig. 10.

The power output plots show a good agreement between theory and the model. The uncertainty in power at low levels is due to the model never reaching a (near) steady state. The resonance frequency has been compared with eqn. 4 in Reference 29 and shows that the model gives a consistently low result. This is thought to be due to the large signal nature of the model.

The turn-on delay has been defined as the time for the carrier concentration to rise from transparency level to threshold level, the same as Thompson's definition [30] of delay time, and is consistent with theory.

The threshold carrier density, which is reached after the transient, has also been examined. In all cases this is within 1% of the expected value. Thus the model appears to be correct in terms of the transient response.

can also cope with inhomogeneous carrier concentration along the cavity length, provided that diffusion is insignificant.

The model is a useful design tool in its present form. However, other multiple rate-equation models [7-10] are able to achieve the same type of results. The justification for this model is that because it is such a close analogue to the laser device, it may be easily modified and enhanced. For example, the next logical addition would be a diffusion model. This would allow the modelling of low facet reflectivity lasers, which have a large photon density distribution along them. Indeed, the modelling of laser amplifiers is then simply a matter of injecting an optical signal into the model.

The above variations have already been tested by the author, but were felt to be beyond the scope of this introductory paper. There are others, one being the extension of the model to two dimensions. Such a model could display transverse, as well as longitudinal, mode hopping and would be essential for gain guided lasers. It would also provide the field distribution across the cavity,

without having to resort to an effective field/index method.

The complexity of any model is limited by computation time. This model has the distinct advantage that

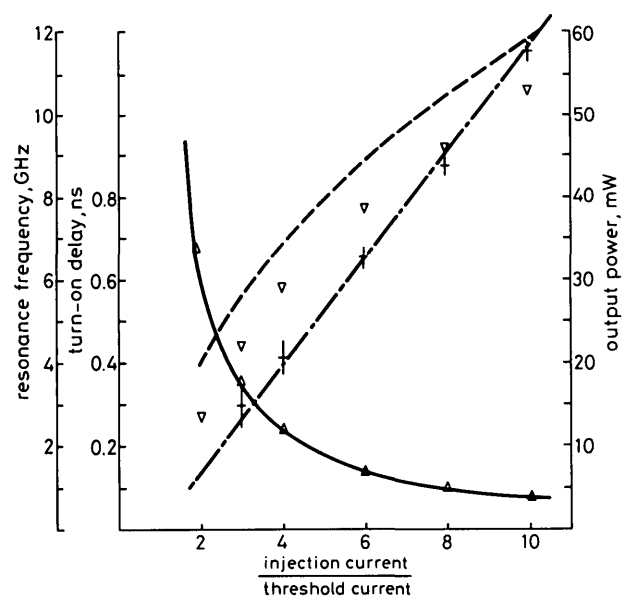


Fig. 10 Output power, resonance frequency and turn-on delay against injection current

— · — · — output power theory, + model
 - - - - - resonance frequency theory, ∇ model
 — — — — — turn-on delay theory, Δ model

accuracy may be compromised for speed in a predictable manner. This allows the model to be used for rough predictions, as well as for accurate analysis. This feature is invaluable in a computer-aided design package, where a number of designs may be quickly compared before one is finally evaluated. For example, the model may be used with very few sections if the bandwidth of the gain peak is made sufficiently narrow. The model is then effectively reduced to a single-frequency rate-equation model.

13 Conclusion

Frequency-selective gain networks have been added to a 1D transmission-line model (TLM) of the field in a laser cavity to produce a transmission-line laser model (TLLM). A technique of sampling below the optical frequency has been introduced to allow a 1 ns transient to be modelled in a realistic time. The results show the evolution of output spectra and are in good agreement with those from a small signal analysis of the rate equations.

14 References

- 1 BUUS, J.: 'Principles of semiconductor laser modelling', *IEE Proc. J, Optoelectron.*, 1985, **132**, (1), pp. 42–51
- 2 HAKKI, B.W.: 'GaAs double heterostructure lasing behaviour along the junction plane', *J. Appl. Phys.*, 1975, **46**, pp. 292–302
- 3 HENRY, C.H.: 'Theory of the linewidth of semiconductor lasers', *IEEE J. Quantum Electron.*, 1982, **QE-18**, pp. 259–264

- 4 JOHNS, P.B.: 'Application of the transmission-line-matrix method to homogeneous waveguides of arbitrary cross-section', *Proc. IEE*, 1972, **119**, pp. 1086–1091
- 5 COGAN, D.DE, and JOHN, S.A.: 'A two-dimensional transmission line matrix model for heat flow in power semiconductors', *J. Phys. D*, 1985, **18**, pp. 507–516
- 6 HENRY, P.S.: 'Lightwave primer', *IEEE J. Quantum Electron.*, 1985, **QE-21**, pp. 1862–1879
- 7 ADAMS, M.J., and OSINSKI, M.: 'Longitudinal mode competition in semiconductor lasers; rate equations revisited', *IEE Proc. I, Solid-State & Electron Dev.*, 1982, **129**, (6), pp. 271–274
- 8 OTSUKA, K., and TARUCHA, S.: 'Theoretical studies on injection locking and injection induced modulation of laser diodes', *IEEE J. Quantum Electron.*, 1981, **QE-17**, pp. 1515–1521
- 9 MARCUSE, D., and LEE, T.-P.: 'On approximate analytical solutions of rate equations for studying transient spectra of injection lasers', *ibid.*, 1983, **QE-19**, pp. 1397–1406
- 10 PETERMANN, K.: 'Theoretical analysis of spectral modulation behaviour of semiconductor injection lasers', *Opt. & Quantum Electron.*, 1978, **10**, pp. 233–242
- 11 OSINSKI, M., and ADAMS, M.J.: 'Transient time-averaged spectra of rapidly-modulated semiconductor lasers', *IEE Proc. J, Optoelectron.*, 1985, **132**, (1), pp. 34–37
- 12 TUCKER, R.S.: 'High-speed modulation of semiconductor lasers', *J. Lightwave Technol.*, 1985, **LT-3**, pp. 1180–1192
- 13 JOHNS, P.B., and O'BRIEN, M.: 'Use of the transmission-line modelling (TLM) method to solve non-linear lumped networks', *Radio & Electron Eng.*, 1980, **50**, pp. 59–70
- 14 KRESSEL, H., and BUTLER, J.: 'Semiconductor lasers and hetero-junction LEDs' (Academic Press, New York, 1977)
- 15 CHEN, K.-L., and WANG, S.: 'An approximate expression for the effective refractive index in symmetric DH lasers', *IEEE J. Quantum Electron.*, 1983, **QE-19**, pp. 1354–1356
- 16 JOHNS, P.B., and BEURLE, R.L.: 'Numerical solution of 2-dimensional scattering problems using a transmission-line matrix', *Proc. IEE*, 1971, **118**, pp. 1203–1208
- 17 NYQUIST, H.: 'Certain topics in telegraph transmission theory', *Trans. Am. Inst. Electr. Eng.*, 1928, **47**, pp. 617–644
- 18 JOHNS, P.B.: 'The solution of inhomogeneous waveguide problems using a transmission line matrix', *IEEE Trans.*, 1974, **MTT-22**, pp. 209–215
- 19 BUUS, J.: 'Analytical approximation for the reflectivity of DH lasers', *IEEE J. Quantum Electron.*, 1981, **QE-17**, pp. 2256–2257
- 20 STATZ, H., and DE MARS, G.: 'Transient and oscillation pulses in masers', in Townes, C.H. (Ed.): 'Quantum electronics' (Columbia Press, New York, 1960), pp. 530–537
- 21 STERN, F.: 'Calculated spectral dependence of gain in excited GaAs', *J. Appl. Phys.*, 1976, **47**, pp. 5382–5386
- 22 MENDOZA-ALVAREZ, J.E., NUNES, F.D., and PATEL, N.B.: 'Refractive index dependence on free carriers for GaAs', *ibid.*, 1980, **51**, pp. 4365–4367
- 23 HENRY, C.H., LOGAN, R.A., and BERTNESS, K.A.: 'Spectral dependence of the change in refractive index due to carrier injection in GaAs lasers', *ibid.*, 1981, **52**, pp. 4457–4461
- 24 LAU, K.Y., and YARIV, A.: 'A theory of longitudinal modes in semiconductor lasers', *Appl. Phys. Lett.*, 1982, **40**, pp. 763–765
- 25 LOUDON, R.: 'The quantum theory of light' (Oxford University Press, 1973), pp. 64–69
- 26 WESTBROOK, L.D.: 'Measurements of dg/dN and dn/dN and their dependence on photon energy in $\lambda = 1.5 \mu\text{m}$ InGaAsP laser diodes', *IEE Proc. J, Optoelectron.*, 1986, **133**, (2), pp. 135–142
- 27 JOHNS, P.B.: 'A simple explicit and unconditionally stable numerical routine for the solution of the diffusion equation', *J. Numerical Methods in Engineering*, 1977, **11**, pp. 1307–1328
- 28 YARIV, A.: 'Optical electronics' (Holt Rinehart & Winston, New York, 1985), pp. 474–494
- 29 LAU, K.Y., and YARIV, A.: 'Ultra-high speed semiconductor lasers', *IEEE J. Quantum Electron.*, 1985, **QE-21**, pp. 121–137
- 30 THOMPSON, G.H.B.: 'Physics of semiconductor laser devices' (Wiley, New York, 1980), pp. 165–239



NONLINEAR OPTICAL WAVEGUIDES AND ADVANCED FIBRE DEVICES

A special issue of IEE Proceedings, Part J, June 1987

This special issue arises from a two day meeting held at Savoy Place, London, in May 1986. That meeting was, in turn, organised and stimulated by the JOERS (Joint Optoelectronics Research Scheme) programme 'Advanced Fibre Waveguide Devices'. The majority of the papers in this issue are more complete and updated versions of presentations at the meeting. There are, however, several contributions submitted independently of the meeting. The original concept of both the meeting and the special issue was to bring together work on nonlinear effects in waveguides, in particular optical fibres, and developments in advanced fibre devices. This issue has been arranged to bring out this link.

Contents

- Nonlinear effects in optical fibres and fibre devices
- Reducing soliton interaction in single-mode optical fibres
- Surface-guided nonlinear TM waves in planar waveguides
- Observation of stimulated Raman scattering and nonlinear pulse broadening at 1.32 μm in monomode optical fibres
- Spectral and temporal investigation of self-phase modulation and stimulated Raman scattering in a single-mode optical fibre
- Optical pulse compression of Raman-depleted picosecond pulses and spectrally windowed self-phase modulated pulses at 1.06 μm
- Investigation of nonlinear power transmission limits in optical-fibre devices
- Q-switching, mode-locking and tunable operation around 0.9 μm of a neodymium-doped monomode fibre laser
- Low-threshold operation of a waveguide CH_4 Raman laser at 1.54 μm
- Concatenated, tapered coaxial coupler filters
- High-reflectivity surface-relief gratings in single-mode optical fibres
- Compact all-fibre Mach-Zehnder devices

Bibliographic details: *IEE Proceedings, Vol. 134, Pt. J, No. 3, June 1987*
UK ISSN: 0267 3932



ORDER FORM

To: The Institution of Electrical Engineers, PO Box 26, Hitchin, Herts SG5 1SA, United Kingdom. Tel: 0462 53331

Please send copy/copies of the Nonlinear Optical Waveguides and Advanced Fibre Devices special issue of IEE Proceedings, Part J, at £17.00 each.

[IEE Members may each purchase one copy for their own use for only £7.00 provided that payment accompanies the order, IEE membership number should be clearly stated.]

Credit card orders (Access and Visa) are considered prepaid and will be accepted by telephone on 0462 53331. Invoices for orders that are not prepaid will include a handling and package charge of £1.50 per issue (maximum £6.00).

Cheque enclosed for £ Cheques drawn on non-UK banks should be in the currency of the country of the bank.

Or Please debit my ACCESS/VISA Card No.

Expiry date Signature

Or purchase order no. IEE Membership No. (if applicable)

Signature Date

Name
BLOCK CAPITALS

Address

.....

